



## Oxidation of $Ti_{n+1}AlX_n$ ( $n = 1-3$ and $X = C, N$ )

### II. Experimental Results

M. W. Barsoum, N. Tzenov, A. Procopio, T. El-Raghy, and M. Ali

Department of Materials Engineering, Drexel University, Philadelphia, Pennsylvania 19104, USA

In this, Part II of a two-part study, the oxidation kinetics in air of the ternary compounds  $Ti_2AlC$ ,  $Ti_2AlC_{0.5}N_{0.5}$ ,  $Ti_4AlN_{2.9}$ , and  $Ti_3AlC_2$  are reported. For the first two compounds, in the 1000-1100°C temperature range and for short times ( $\approx 20$  h) the oxidation kinetics are parabolic. The parabolic rate constants are  $k_x$  ( $m^2/s$ ) =  $2.68 \times 10^5 \exp - 491.5$  (kJ/mol)/ $RT$  for  $Ti_2AlC$ , and  $2.55 \times 10^5 \exp - 458.7$  (kJ/mol)/ $RT$  for  $Ti_2AlC_{0.5}N_{0.5}$ . At 900°C, the kinetics are quasi-linear, and up to 100 h the outermost layers that form are almost pure rutile, dense, and protective. For the second pair, at short times ( $< 10$  h) the oxidation kinetics are parabolic at all temperatures examined (800-1100°C), but become linear at longer times. The  $k_x$  values are  $3.2 \times 10^5 \exp - 429$  (kJ/mol)/ $RT$ , for  $Ti_4AlN_{2.9}$  and  $1.15 \times 10^5 \exp - 443$  (kJ/mol)/ $RT$  for  $Ti_3AlC_2$ . In all cases, the scales that form are comprised mainly of a rutile-based solid solution,  $(Ti_{1-y}Al_y)O_{2-y/2}$  where  $y < 0.05$ , and some  $Al_2O_3$ . The oxidation occurs by the inward diffusion of oxygen and the outward diffusion of Al and Ti. The C and N atoms are presumed to also diffuse outward through the oxide layer. At the low oxygen partial pressure side, the  $Al^{3+}$  ions dissolve in and diffuse through the  $(Ti_{1-y}Al_y)O_{2-y/2}$  layer and react with oxygen to form  $Al_2O_3$  at the high oxygen pressure side. This demixing results in the formation of pores that concentrate along planes, especially at longer times and higher temperatures. These layers of porosity impede the diffusion of Al, but not those of Ti and oxygen, which results in the formation of highly striated scales where three layers, an  $Al_2O_3$ -rich, a  $TiO_2$ -rich, and a porous layer repeat multiple ( $> 10$ ) times. The presence of oxygen also reduces the decomposition (into  $TiX_x$  and Al) temperatures of  $Ti_4AlN_{2.9}$  and  $Ti_3AlC_2$  from a  $T > 1400^\circ C$ , to one less than  $1100^\circ C$ .  
© 2001 The Electrochemical Society. [DOI: 10.1149/1.1380256] All rights reserved.

Manuscript submitted July 26, 2000; revised manuscript received February 6, 2001. Available electronically July 9, 2001.

In this, Part II of a two-part study,<sup>1</sup> we report on the oxidation in air in the 800-1100°C temperature range, of the ternary compounds  $Ti_2AlC$ ,  $Ti_2AlC_{0.5}N_{0.5}$ ,  $Ti_4AlN_{2.9}$ , and  $Ti_3AlC_2$ . Since this is the first report on the oxidation of these compounds, there are no previous results with which to compare; it is thus instructive to review the oxidation behavior of some related solids such as Ti, and some Ti-aluminides such as TiAl,  $Ti_3Al$ , and “ $Ti_2Al$ ,” which is a two-phase mixture of the first two. The oxidation of  $Ti_3SiC_2$ <sup>2</sup> was briefly reviewed in Part I.<sup>1</sup>

The oxidation of pure Ti in the 600-1000°C temperature range is parabolic.<sup>3-7</sup> In this temperature range, individual rutile  $TiO_2$  layers form that range in thickness from 1 to 8  $\mu m$  depending inversely on temperature.<sup>3-7</sup> These stratified layers tend to spall off periodically. Simultaneously with the formation of a  $TiO_2$  scale, substantial amounts of oxygen dissolve in the Ti substrate. The same is true for the Ti-aluminides; most, but especially the ones for which the Ti:Al ratio is around 2:1, dissolve substantial amounts of oxygen (see below).

It is well established that the oxidation behavior of Ti-Al intermetallics is strongly dependent on the aluminum content.<sup>8-13</sup> Typically,  $\sim 60$  to 70 atom % Al is required in binary Ti-Al alloys to form continuous alumina,  $Al_2O_3$  scales in air.<sup>9</sup> In pure oxygen, the Al content needed is lower.<sup>9,10</sup> For concentrations that are less than 50 atom %, both  $TiO_2$  and  $Al_2O_3$  form.<sup>8-11</sup> The scale morphologies that form are similar to the ones observed in this work, namely, stratified multilayer scales. The layers that form, from the outside in, are typically  $TiO_2$ / $Al_2O_3$ -rich layer/ $TiO_2$  +  $Al_2O_3$ /internal oxides.

In general, the oxidation resistance of  $Ti_3Al$  in air, or oxygen, is quite poor at temperatures greater than 850°C.<sup>9-13</sup> At lower temperatures and shorter time, the scales, predominately composed of  $TiO_2$ , are adherent. Above 850°C, the scales tend to be loosely adherent and spall off. Roy *et al.*<sup>12</sup> have shown that the oxidation kinetics in the 725-1025°C temperature range, especially at short times ( $< 5$  h), are reasonably well described by a parabolic law. The authors also noted that the oxidation resulted in a scale in which thin  $Al_2O_3$ -rich layers alternate with  $TiO_2$  layers; a layering that introduced porosity in the reaction scales. Welsch and Kahveci<sup>9</sup> have shown that when a Ti-26 atom % Al sample is oxidized in dry oxygen, four layers formed: an external  $TiO_2$  layer, followed by an  $Al_2O_3$ -rich layer

(balance  $TiO_2$ ), followed by a  $TiO_2$ -rich (balance  $Al_2O_3$ ) layer. This, in turn, is followed by an O embrittled alloy layer.

Since the ternary compounds studied in this work do not dissolve oxygen, comparing the parabolic rate constants calculated from weight gain measurements,  $k_w$ , with those calculated from oxide film thicknesses,  $k_x$ , is problematic. To circumvent this problem, the  $k_x$  values reported in this paper taken from the literature were calculated directly from micrographs shown in the various references and/or when the thicknesses of the oxide layers when explicitly given. For example, Unnan *et al.*<sup>7</sup> measured the  $TiO_2$  film thicknesses on commercial Ti after their exposure in air in the 593-760°C temperature range and deduced that<sup>a</sup>

$$k_x \text{ (m}^2\text{/s)} = 1.4 \times 10^{-4} \exp - 231,176 \text{ (kJ/mol)/}RT \quad [1]$$

The aim of this paper is to report on the oxidation behavior of  $Ti_2AlC$ ,  $Ti_2AlC_{0.5}N_{0.5}$ ,  $Ti_3AlC_2$ , and  $Ti_4AlN_{2.9}$  in air in the 800-1100°C temperature range. The results are discussed in light of the model presented in Part I<sup>1</sup> and compared to those of relevant Ti-aluminide intermetallics.

### Experimental

All of the samples were fabricated by reactively hot isostatically pressing, various powder mixture combinations of Ti,  $TiH_2$ ,  $Al_4C_3$ , C, AlN, and/or TiN to yield the desired stoichiometries. The sources and purities of the powders used in this work are listed in Table I. The processing details can be found elsewhere.<sup>14-16</sup>

For the  $Ti_2AlC_{0.5}N_{0.5}$  and  $Ti_2AlC$  phases, henceforth referred to as the 211 phases, the powders were mixed, cold pressed, and sealed under vacuum in Pyrex tubes. The latter were then placed in a hot isostatic press, and heated at 10°C/min to 850°C and held at that temperature for 30 min. The chamber was pressurized with Ar to  $\approx 25$  MPa, the heating resumed at the initial rate, at which time the pressure increased to  $\approx 40$  MPa. The  $Ti_2AlC_{0.5}N_{0.5}$  and  $Ti_2AlC$  samples were processed at 1300°C for 15 and 30 h, respectively. The final grain sizes were of the order of 23  $\mu m$  in both cases. The

<sup>a</sup> This expression is calculated from Eq. 11 in Ref. 7, and includes the factor of 2 used in Eq. 4 in the definition of  $k_x$ .

**Table I. Characteristics and sources of powders used in this work.**

Powder	Purity (%)	Particle size	Source	Composition in wt % <sup>a</sup>
Ti	99.46	-325 mesh	Ti Powder Specialists, Sandy, UT	C = 0.03, Fe = 0.04, Si = 0.02, N = 0.03, O = 0.17, Cl = 0.12, H = 0.034
TiH <sub>2</sub> for Ti <sub>4</sub> AlN <sub>3</sub>	99.3	-325	Timet, Henderson, NV	
C	99	$d_m = 1-2 \mu\text{m}$	Aldrich Chemical, Milwaukee, WI	
Al <sub>4</sub> C <sub>3</sub> for Ti <sub>3</sub> AlC <sub>2</sub>	99	-325	Cerac, Milwaukee, WI	
Al <sub>4</sub> C <sub>3</sub> for 211	99.7	$d_m = 10 \mu\text{m}$	Alpha Aesar, Ward Hill, MA	C = 25.57; Ca, Cu, Mn, Ti, Ni, V, Zr < 0.01; Co = 0.09; Fe = 0.08; Cr = 0.04; Mg < 0.001; Si = 0.1
TiN	99.8	2.5-4 $\mu\text{m}$	Alfa Aesar, Ward Hill, MA	N = 32% minimum
AlN	98.9	$d_m = 3.8 \mu\text{m}$	Alpha Aesar, Ward Hill, MA	N = 33.2, O = 1.1, C = 0.08, Fe = 0.09

<sup>a</sup> According to manufacturers specifications.

samples were fully dense and predominantly single phase. In both cases,  $\approx 4$  vol % impurity phases that contained O and P were detected. More details can be found in Ref. 14.

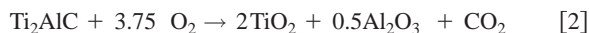
To fabricate the Ti<sub>3</sub>Al<sub>1.1</sub>C<sub>1.8</sub> samples, Ti, Al<sub>4</sub>C<sub>3</sub>, and C were mixed to yield a final stoichiometry of Ti<sub>3</sub>Al<sub>1.1</sub>C<sub>1.8</sub>. The green bodies were sealed under vacuum and hot isostatically pressed (HIP) at 1400°C for 16 h under a pressure of  $\approx 70$  MPa. The final grain size was of the order of 30  $\mu\text{m}$ . The samples were fully dense, and predominantly single phase, with  $\approx 4$  vol % of Al<sub>2</sub>O<sub>3</sub> as an impurity phase. Further details can be found in Ref. 15. Recent microprobe analysis of this composition indicated that the final chemistry is Ti<sub>3</sub>AlC<sub>2</sub>.

The processing details for the Ti<sub>4</sub>AlN<sub>2.9</sub> samples are described elsewhere.<sup>16</sup> In brief powder compacts of TiH<sub>2</sub>, TiN and AlN were mixed, dehydrated, and reactively HIP at 1275°C for 24 h under a pressure of 70 MPa. This was followed by a further anneal in Ar at 1360°C for 168 h. Phase analysis showed TiN and Al<sub>2</sub>O<sub>3</sub> were present in minor amounts.<sup>16</sup> The measured density was  $\approx 0.95$  of theoretical (4.77 g/cm<sup>3</sup>) and the grains were in the 20 to 30  $\mu\text{m}$  range.<sup>6</sup>

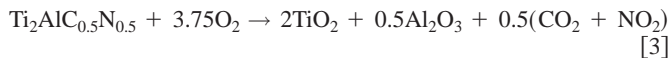
Prior to the oxidation runs, the samples were rough polished using 600 grit SiC grinding paper, placed on a Pt mesh, heated to the oxidation temperature at 10°C/min for a predetermined time, and furnace cooled. The oxide layer thicknesses were measured in a scanning electron microscope (SEM) (Amray 1830), equipped with an energy dispersive spectroscopy (EDS) system for chemical analysis (LINK ISIS, Oxford Instruments, England). The phases formed upon oxidation were determined from X-ray diffraction (XRD) spectra of crushed surface layers.

### Results and Discussion

*Ti<sub>2</sub>AlC and Ti<sub>2</sub>AlC<sub>0.5</sub>N<sub>0.5</sub>*.—The XRD spectra of the layers that form as a result of the oxidation of Ti<sub>2</sub>AlC and Ti<sub>2</sub>AlC<sub>0.5</sub>N<sub>0.5</sub> in air at 1100°C, for 4 h are shown in Fig. 1. The major peaks correspond to TiO<sub>2</sub> and Al<sub>2</sub>O<sub>3</sub>, with the intensity of the former being greater. No evidence for titanium aluminate was found even after oxidation at 1100°C for long times. Similar XRD patterns were found at the other temperatures as well. Based on these results, the most likely overall oxidation reaction for Ti<sub>2</sub>AlC is



Similarly, for the solid solution



These reactions assume that the nonmetallic elements diffuse through the reaction layers and oxidize. The exact nature of the gas that forms is unknown at this time; the assumption that they are NO<sub>2</sub> and/or CO<sub>2</sub> is made here in order to balance the reactions.

The molar volumes of Ti<sub>2</sub>AlC,<sup>14</sup> Ti<sub>2</sub>AlC<sub>0.5</sub>N<sub>0.5</sub>,<sup>14</sup> TiO<sub>2</sub>, and Al<sub>2</sub>O<sub>3</sub> are 32.86, 32.32, 18.57, and 26.14 cm<sup>3</sup>/mol. Thus, the volume changes for Reactions 2 and 3 are +193 and +196%, respectively. It is thus not surprising that the oxide layers that form are, for the most part, dense and protective.

The time,  $t$ , dependencies of the oxide layer thicknesses,  $x$ , that form on Ti<sub>2</sub>AlC and Ti<sub>2</sub>AlC<sub>0.5</sub>N<sub>0.5</sub> at various temperatures are plotted in Fig. 2a and 3a, respectively. A comparison of the two figures indicates that Ti<sub>2</sub>AlC is more susceptible to oxidation than Ti<sub>2</sub>AlC<sub>0.5</sub>N<sub>0.5</sub>. The exponent,  $n$ , of the best power law fit to time, *i.e.*,  $t^n$ , is shown on the graphs.<sup>b</sup> From these values of  $n$ , one can conclude that at 900°C, the oxidation kinetics are neither parabolic nor linear, but that at the higher temperatures, the kinetics are parabolic for both compounds. This was verified by plotting the thickness squared vs.  $t$  (Fig. 2b and 3b). The parabolic rate constants,  $k_x$ , were fit to the expression

<sup>b</sup> The exponents were determined from log-log plots of  $x$  vs.  $t$ . Once the exponents were determined, they were used to draw the lines shown in Fig. 2a and 3a.

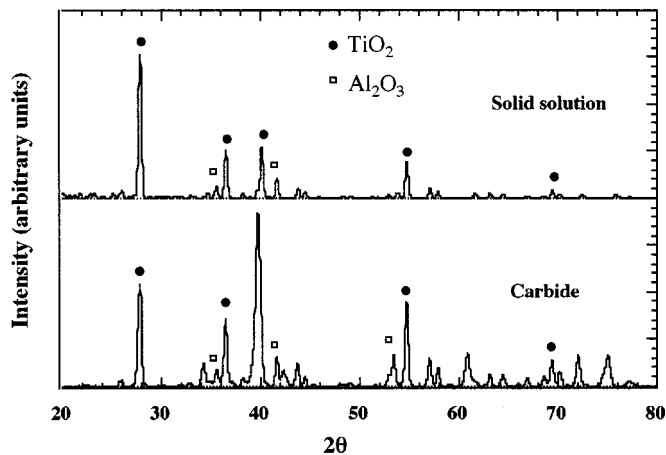


**Figure 1.** XRD spectra of reaction layers that form on oxidation of Ti<sub>2</sub>AlC and Ti<sub>2</sub>AlC<sub>0.5</sub>N<sub>0.5</sub> in air at 1100°C for 64 h. (●) rutile peaks, (□) Al<sub>2</sub>O<sub>3</sub>.

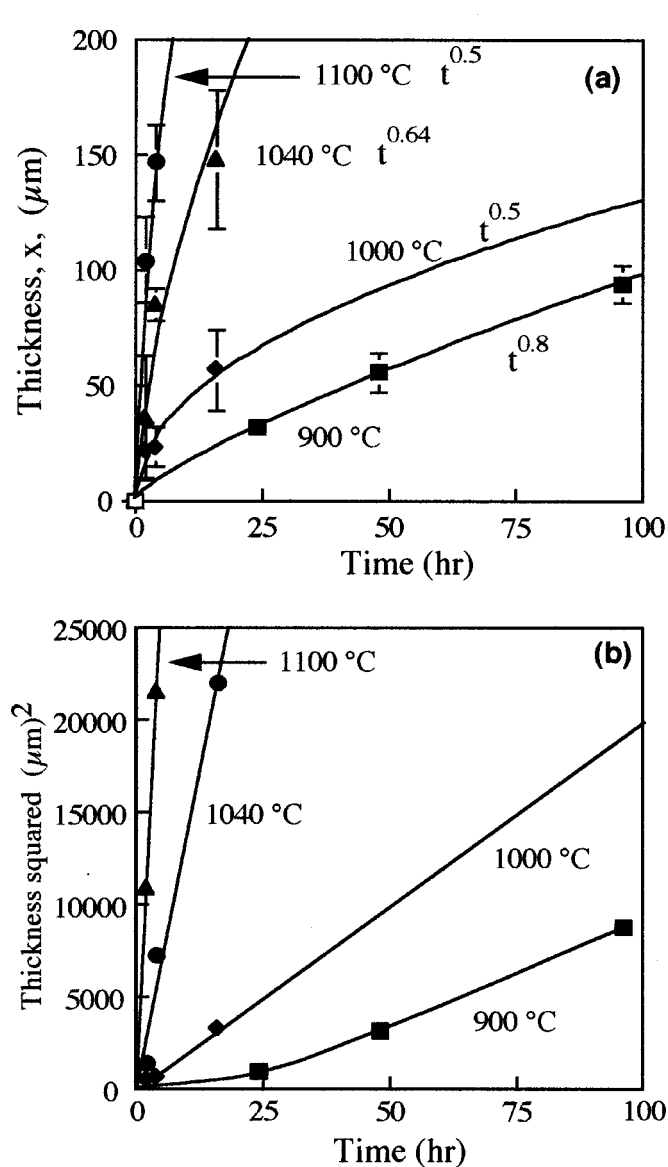


**Figure 2.** Time dependence of oxide thickness,  $x$ , formed on  $\text{Ti}_2\text{AlC}$  samples as a function of temperature and plotted as (a)  $x$  vs.  $t$ . Solid lines are plots of  $x = Kt^n$ , where  $n$  was determined from least-squares fits of  $\log x$  vs.  $\log t$  plots; (b)  $x^2$  vs.  $t$ . Typical error bars are shown.

$$x^2 = 2k_x t \quad [4]$$

The results are listed in Table I in Part I.<sup>1</sup> Arrhenius plots of  $k_x$  for  $\text{Ti}_2\text{AlC}$  and  $\text{Ti}_2\text{AlC}_{0.5}\text{N}_{0.5}$  are shown in Fig. 4a. A least-squares fit of the experimental results yields

$$k_x \text{ (m}^2\text{/s)} = 2.55 \times 10^5 \exp - 458,766/RT \quad [5]$$

for  $\text{Ti}_2\text{AlC}$ , and

$$k_x \text{ (m}^2\text{/s)} = 2.68 \times 10^6 \exp - 491,515/RT \quad [6]$$

for  $\text{Ti}_2\text{AlC}_{0.5}\text{N}_{0.5}$ . The corresponding activation energies are 458.7 and 491.5 kJ/mol. Also included in Fig. 4a are the  $k_x$  values for the oxidation of  $\text{Ti}^7$  (Eq. 1),  $\text{Ti}_2\text{Al}$ ,<sup>8,9</sup> and  $\text{TiAl}$ .<sup>9,11</sup> Not surprisingly, the  $k_x$  values of the ternaries are comparable to those of the intermetallics.

A typical backscattered SEM micrograph of the cross section of a  $\text{Ti}_2\text{AlC}_{0.5}\text{N}_{0.5}$  sample oxidized at 1040°C for 16 h is shown in Fig.

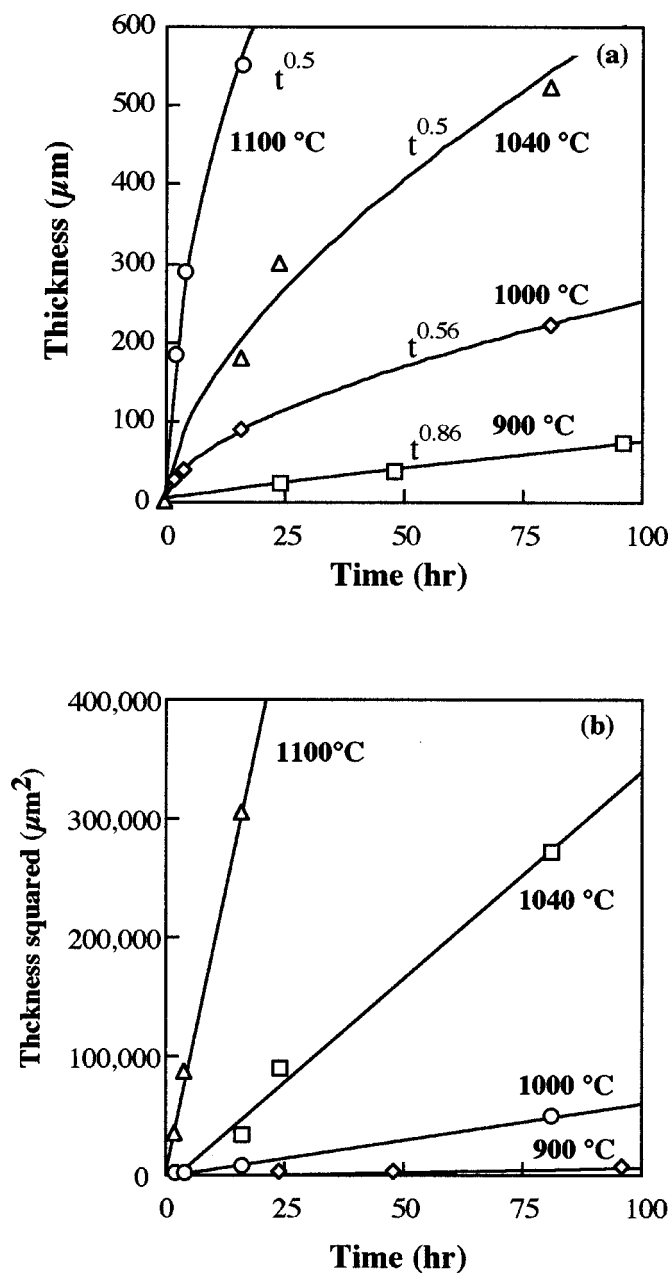


**Figure 3.** Time dependence of oxide thickness,  $x$ , formed on  $\text{Ti}_2\text{AlC}_{0.5}\text{N}_{0.5}$  samples as a function of temperature and plotted as (a)  $x$  vs.  $t$ . Solid lines are plots of  $x = Kt^n$ , where  $n$  was determined from least-squares fits of  $\log x$  vs.  $\log t$  plots; (b)  $x^2$  vs.  $t$ .

5 (denoted by corner arrows). The original sharp corners of the sample are clearly visible and decorated by  $\text{Al}_2\text{O}_3$ . Four layers can be identified. An external layer that EDS indicates is  $\text{TiO}_2$ , in which some  $\text{Al}_2\text{O}_3$  stringers are apparent. A thin darker layer that contains some  $\text{TiO}_2$ , but has a high volume fraction of  $\text{Al}_2\text{O}_3$  follows. The next layer is mostly  $\text{TiO}_2$ , in which some  $\text{Al}^{3+}$  ions are dissolved, *i.e.*,  $(\text{Ti}_{1-y}\text{Al}_y)\text{O}_{2-y/2}$  with  $y < 0.05$ . An innermost layer, which is slightly darker and has the appearance of a stain, is once again a two-phase mixture of  $\text{Al}_2\text{O}_3$  and  $(\text{Ti}_{1-y}\text{Al}_y)\text{O}_{2-y/2}$ , but at a finer scale than the previous  $\text{Al}_2\text{O}_3$ -rich layer. A comparison of the order of the layers and their morphologies indicate that this system is in stage II, described in Part I. The layers correspond, respectively, to layers A through D shown in Fig. 1b in Part I. For the sake of

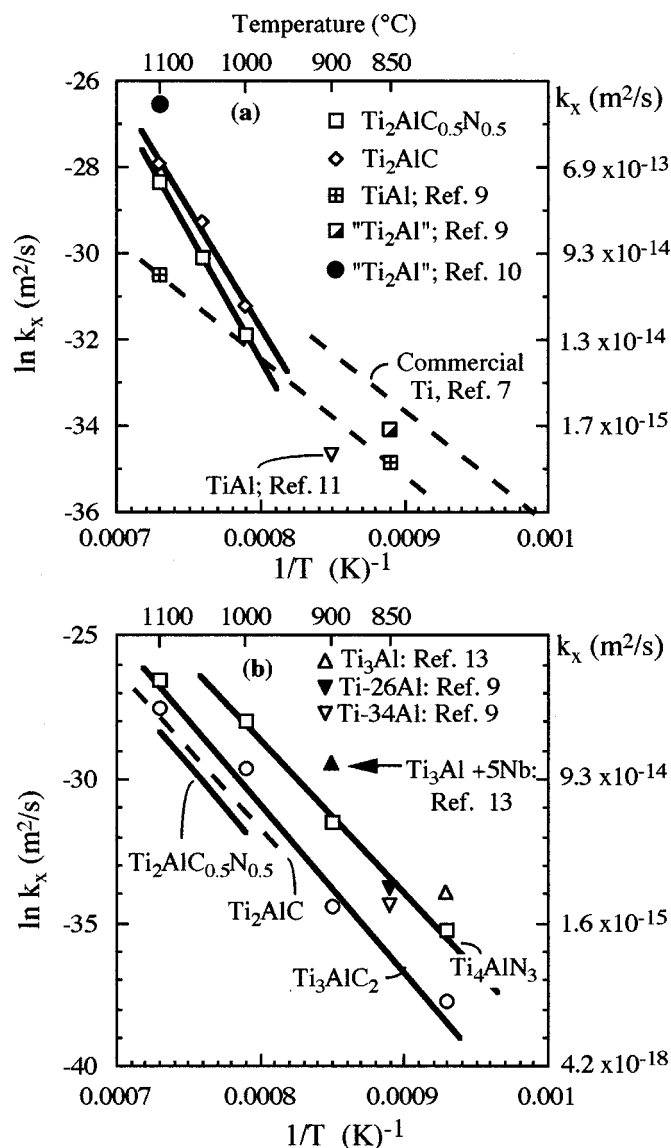


**Figure 4.** Arrhenian plots of parabolic rate constants. (a) For  $\text{Ti}_2\text{AlC}$  and  $\text{Ti}_2\text{AlC}_{0.5}\text{N}_{0.5}$ . Also included in the plot are results for commercial Ti,<sup>7</sup>  $\text{Ti}_2\text{Al}$ ,<sup>9,10</sup>  $\text{TiAl}$ .<sup>11</sup> The  $k_x$  values for the intermetallic compositions were for the most part calculated from micrographs in the original references. (b)  $\text{Ti}_4\text{AlN}_{2.9}$  and  $\text{Ti}_3\text{AlC}_2$ . The data at  $1100^\circ\text{C}$  were excluded from the least-squares fit represented by the bold solid lines. Also included for comparison are the  $k_x$  values obtained from the literature for  $\text{Ti}_3\text{Al}$ <sup>9,13</sup> and the 211's shown in a.

consistency and to avoid confusion the labeling of these layers is identical to the one shown in Fig. 1 in Part I.<sup>1</sup>

Figures 6a and 7a are backscattered SEM micrographs of two  $\text{Ti}_2\text{AlC}_{0.5}\text{N}_{0.5}$  samples oxidized at  $1100^\circ\text{C}$  for 2 and 16 h, respectively. The respective Ti maps are shown in Fig. 6b and 7b; the Al maps in Fig. 6c and 7c. Here again, four layers, A-D, are clearly distinguishable. Comparing the two sets of micrographs, the following salient points can be made.

1. Qualitatively, and but for the obvious differences in magnifications, the two sets of micrographs are quite similar.
2. The width of the Al-rich band, layer B, more apparent in Fig. 7c than in 6c, increases from  $\sim 20 \mu\text{m}$  to  $\sim 60 \mu\text{m}$  with increasing time. The same is true of the Al signal; it is stronger at longer times. This could not have occurred without the outward diffusion of  $\text{Al}^{3+}$  ions through the  $\text{TiO}_2$ -rich layer, viz., the C layer.

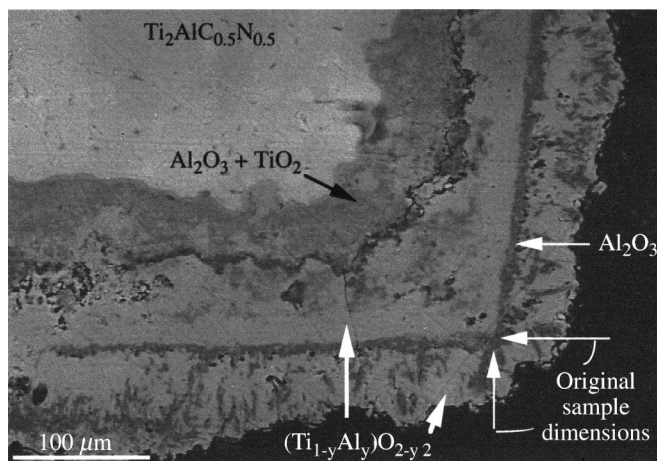


**Figure 5.** Secondary SEM micrographs of  $\text{Ti}_2\text{AlC}_{0.5}\text{N}_{0.5}$  sample oxidized in air at  $1040^\circ\text{C}$  for 16 h. The arrows mark the original sample dimensions. Note that original sharp corners of sample are still visible.

3. The outermost A layers increase in thickness from  $\sim 60$  to  $\sim 180 \mu\text{m}$  with time. This fact alone unambiguously and conclusively proves the Ti ions are diffusing outward. Furthermore, the Al signal in these layers increases substantially with time. Again, this is a result that could not have occurred without the dissolution and reprecipitation of  $\text{Al}^{3+}$  ions within the A layers.

4. Similarly, the layers labeled C and D increase in thickness from  $\sim 100$  to  $\sim 400 \mu\text{m}$ , proving that oxygen diffusion inward is occurring. It is important to point out that layer C does not contain  $\text{Al}_2\text{O}_3$  precipitates. EDS indicates that the Al concentration is low (mole fraction  $\approx 0.01$ ) and more or less constant across this layer. This is compelling evidence for both the outward diffusion of the  $\text{Al}^{3+}$  ions, and their precipitation as  $\text{Al}_2\text{O}_3$  particles at the high oxygen partial pressure side, confirming the notion of demixing discussed in Part I. More compelling evidence for demixing is presented below.

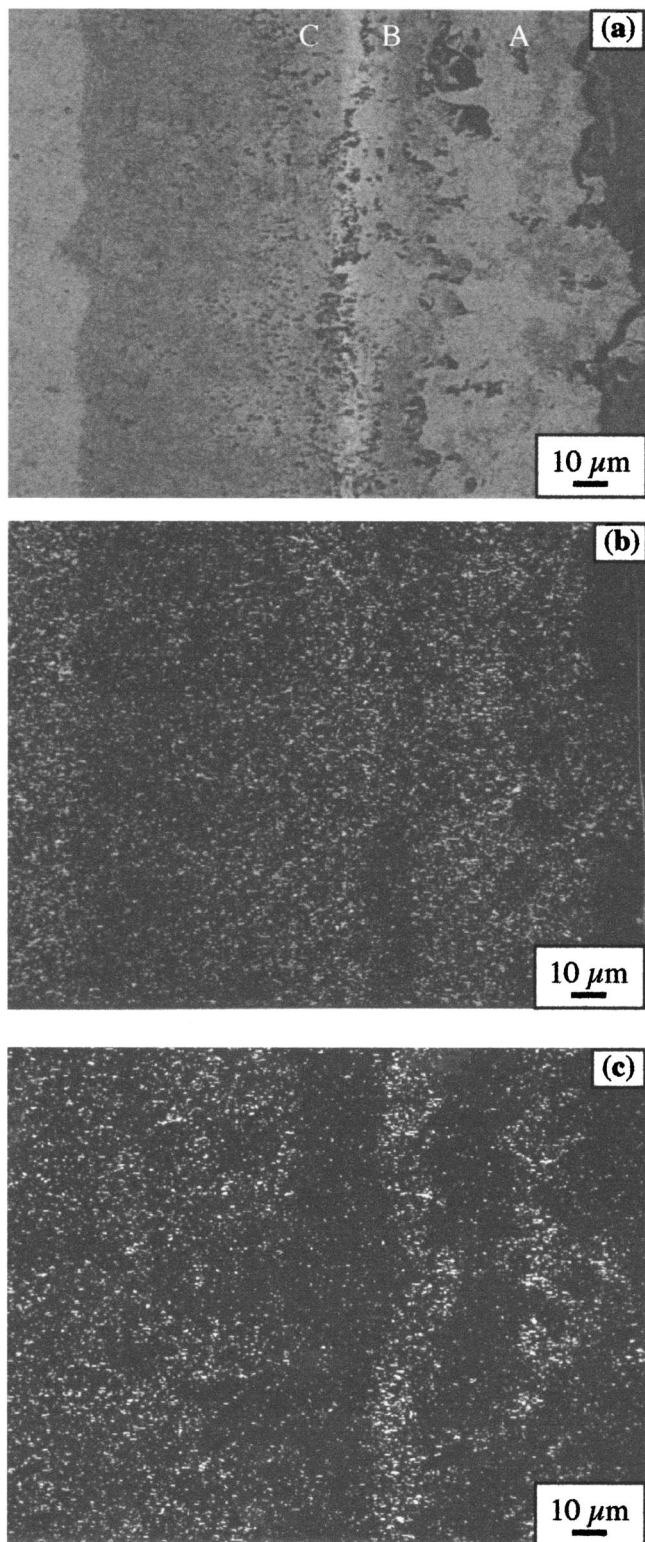
5. The origin of the porosity observed in the micrographs is believed to be the continual outward diffusion of the  $\text{Al}^{3+}$  ions as a result of demixing. More evidence is discussed below.

Figure 8a is a SEM micrograph of a carbide sample oxidized at  $900^\circ\text{C}$  for 96 h. The corresponding Ti and Al maps are shown in Fig. 8b and c, respectively. Qualitatively, there is little difference in the sequence of the layers formed at  $900^\circ\text{C}$  and those formed at  $1100^\circ\text{C}$  (Fig. 6 and 7). The outermost layer at  $900^\circ\text{C}$ , however, has a much weaker Al signal than the ones formed at  $1100^\circ\text{C}$  (compare Fig. 6c or 7c with 8c). Furthermore, at  $900^\circ\text{C}$ , there are no  $\text{Al}_2\text{O}_3$  stringers. Both observations can be taken as indirect evidence that the solubility and/or diffusivity of  $\text{Al}^{3+}$  ions in  $\text{TiO}_2$  is significantly lower at  $900^\circ\text{C}$  than at  $1100^\circ\text{C}$ . As discussed below, Fig. 5-8 can be used to estimate the diffusion coefficients of Al in  $\text{TiO}_2$ .

The SEM micrographs for the oxidized  $\text{Ti}_2\text{AlC}$  samples in the  $900$ - $1100^\circ\text{C}$  temperature range are similar to those shown here for  $\text{Ti}_2\text{AlC}_{0.5}\text{N}_{0.5}$  and are not shown for the sake of brevity.

In comparison of the microstructures shown in Fig. 5 to 8, to the schematic diagram shown in Fig. 1 in Part I,<sup>1</sup> it is clear that in all cases the system is in stage II. In these ternaries, however, the layer of porosity at shorter times either does not form, or, more likely, has sintered shut. The fact that the oxidation kinetics are still parabolic after 80 h (Fig. 3) at  $1040^\circ\text{C}$  indicates that the layer does remain protective. However, at longer times and at the highest temperatures, pores do form.

$\text{Ti}_4\text{AlN}_3$ .—XRD of the reaction scales (not shown) that form



**Figure 6.** Cross-sectional SEM micrographs of a  $\text{Ti}_2\text{AlC}_{0.5}\text{N}_{0.5}$  sample oxidized in air at  $1100^\circ\text{C}$  for 2 h. (a) Backscattered mode, (b) Ti map, (c) Al map.

upon the oxidation of  $\text{Ti}_4\text{AlN}_3$  are similar to those shown in Fig. 1. Based on these results, the most likely overall reaction for the oxidation of  $\text{Ti}_4\text{AlN}_3$  is

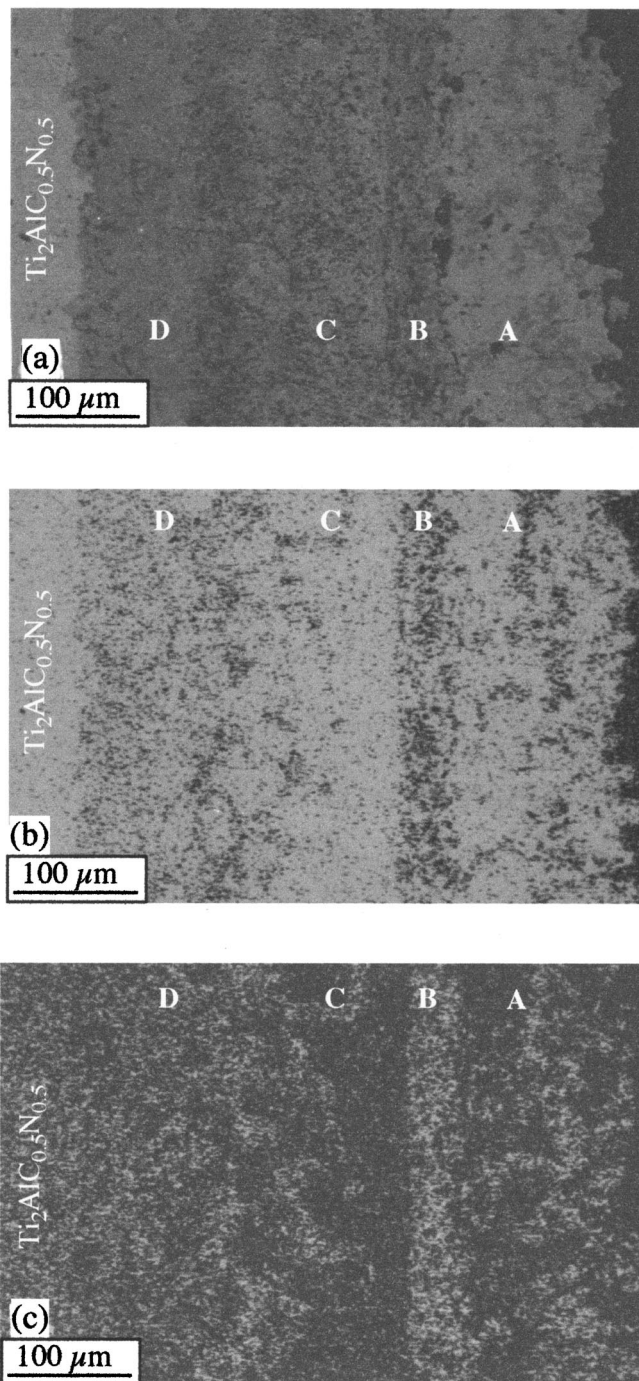


**Figure 7.** Cross-sectional SEM micrographs of a  $\text{Ti}_2\text{AlC}_{0.5}\text{N}_{0.5}$  sample oxidized in air at  $1100^\circ\text{C}$  for 16 h. (a) Backscattered mode, (b) Ti map, (c) Al map.

Here again, the N is assumed to diffuse through the reaction layers and oxidize. The molar volumes of  $\text{Ti}_4\text{AlN}_3$ <sup>16</sup> and  $\text{Ti}_3\text{AlC}_2$ <sup>15</sup> are, respectively,  $61.31$  and  $45.8 \text{ cm}^3/\text{mol}$ . Hence, the volume changes upon oxidation are of the order 150% which, theoretically, should result in a dense and protective scale. The reason that is not the case is discussed below.

The time dependencies of  $x$  that form on  $\text{Ti}_4\text{AlN}_{2.9}$  at various temperatures are plotted in Fig. 9. Initially, and up to about  $\sim 16$  h at  $800$ ,  $900$ , and  $1000^\circ\text{C}$ , and up to  $\sim 9$  h at  $1100^\circ\text{C}$ , the kinetics are reasonably well described by parabolic kinetics. This is shown in Fig. 9a and b by the dotted lines, which were drawn by first least-

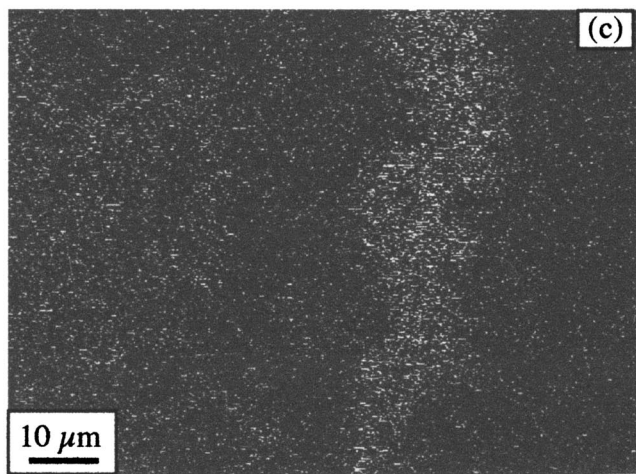
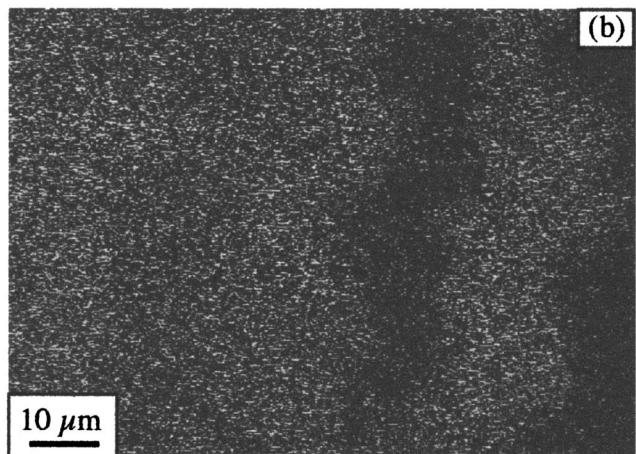
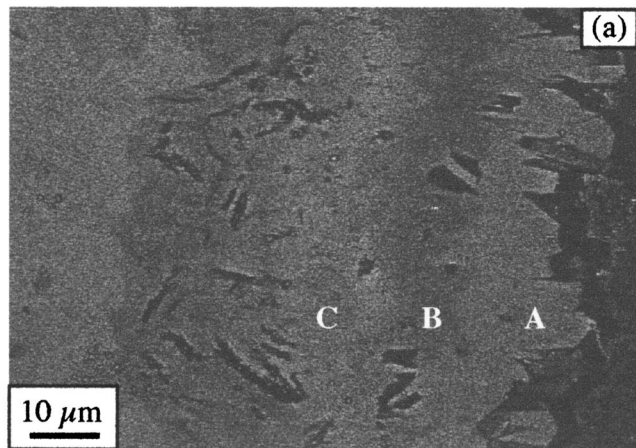


Figure 8. Cross-sectional SEM micrographs of a  $Ti_2AlC_{0.5}N_{0.5}$  sample oxidized in air at  $900^\circ C$  for 96 h. (a) Backscattered mode, (b) Ti map, (c) Al map.

squares fitting  $x^2$  vs.  $t$  plots to determine  $k_x$  at times less than 20 h. Once the  $k_x$  values were determined, the time dependencies of  $x$  were replotted on Fig. 9 as dashed lines. Considering the experimen-

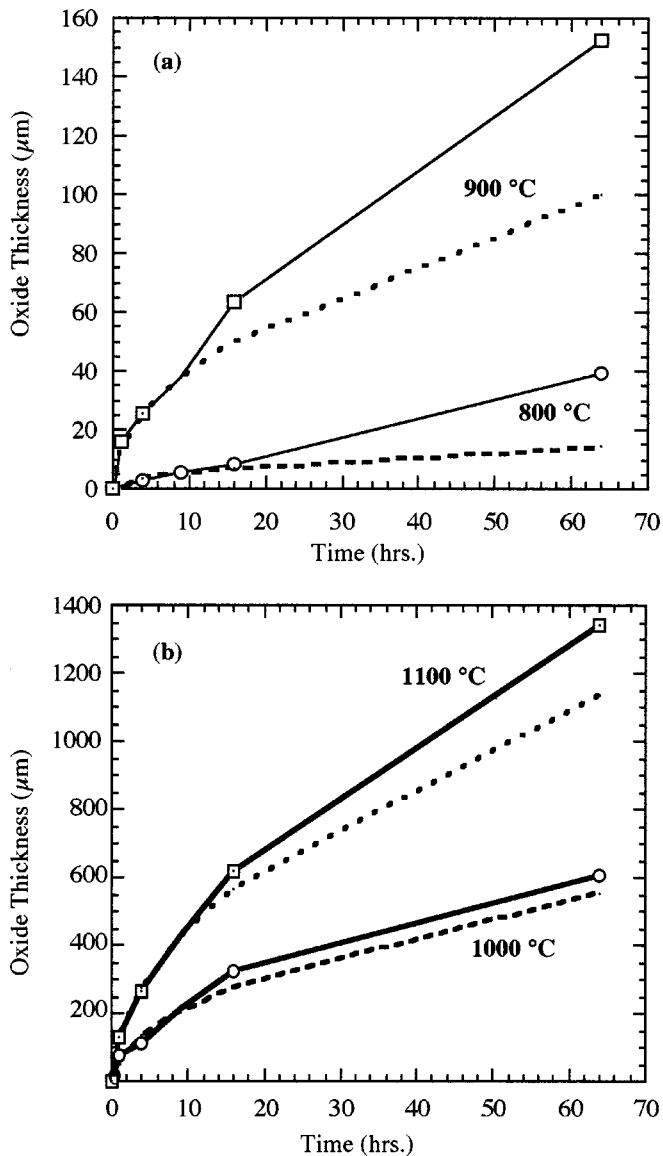


Figure 9. Time dependence of layer thickness,  $x$ , formed on  $Ti_4AlN_{2.9}$  samples oxidized at (a)  $800^\circ C$  and  $900^\circ C$ , and (b)  $1000^\circ C$  and  $1100^\circ C$ . The dashed lines represent Eq. 4 in text, plotted using  $k_x$  values obtained from least-squares fits of  $x^2$  vs.  $t$  curves (not shown) at short times ( $<20$  h).

tal scatter, the agreement between the two sets of results is reasonable, especially at shorter times. At longer times, the kinetics are clearly no longer parabolic, but are more or less linear. It is worth noting that it is possible to obtain a better fit of the results shown in Fig. 9b at longer times, but at the expense of the fits at shorter time. However, since the microstructural observations are more in tune with a system in which the kinetics are parabolic at short times, the analysis described above was adopted. The correction is small, however, and does not affect any of the conclusions reached herein.

A least squares fit of Arrhenius plots of the  $k_x$  results yields the following relationships for  $Ti_4AlN_{2.9}$

$$k_x \text{ (m}^2\text{/s)} = 3.2 \times 10^5 \exp - \frac{429,607 \text{ (kJ/mol)}}{RT} \quad [8]$$

which is plotted in Fig. 4b. For reasons discussed below, namely, the dissociation of  $Ti_4AlN_{2.9}$ , the datum point at  $1100^\circ C$  was excluded from the least-squares fits.

A series of backscattered SEM micrographs all taken at the same magnification, of samples that were oxidized at 900°C for 0.5, 1, and 2 h are shown in Fig. 10a-c, respectively. The following observations are noteworthy.

1. After 0.5 h (Fig. 10a), the oxidized layer is more or less compositionally uniform and is physically separated from the substrate by a gap extending parallel to the substrate/oxide interface. The origin of this gap must be the rapid outward diffusion of the cations. In other words, this gap forms as a result of the coalescence of vacancies resulting from the Kirkendall effect. This feature, in agreement with Part I,<sup>1</sup> is henceforth referred to as the P layer or plane.

2. After 1 h (Fig. 10b), compositional differentiation (where the outermost layer is TiO<sub>2</sub>-rich, followed by an Al<sub>2</sub>O<sub>3</sub>-rich layer followed again by a TiO<sub>2</sub>-rich one followed by a gap) is apparent. These layers correspond, respectively, to layers A, B, C, and P in Part I.<sup>1</sup> The P layer is now wider and has moved inward. The latter observation alone is compelling evidence that sintering must be occurring during the oxidation process. This is best seen by comparing Fig. 10a and b. The gap that formed in Fig. 10a and is still partially visible in Fig. 10b, but is being "filled" by Al<sub>2</sub>O<sub>3</sub> particles must occur by a reaction between the outward diffusing cations and the inward diffusing O<sup>2-</sup> ions. The rapid outward diffusion of the cations leads to the formation of another gap roughly 8 μm below the surface (Fig. 10b).

3. After 2 h (Fig. 10c), not only are the three layers much more clearly defined, but they all have increased in thickness. The original gap formed in Fig. 10a has almost disappeared, and the second gap has gotten wider, and is no longer a clearly defined gap. Instead it is an area of high porosity, which is reminiscent of a collection of particles in the process of sintering. These particles most probably form as a result of a reaction between the inward diffusing O<sup>2-</sup> ions and the outward diffusing cations. However, since the Al diffusion is much more rapid, it tends to concentrate in the B layer nearest the surface. Note that the diffusion of Al in the outermost layer, A, is significantly slower than its diffusion in the C layer. For example, from Fig. 10c, the characteristic diffusion distance for the Al<sup>3+</sup> ions in the C layer is ≈10 μm, in, at most, 2 h. In contradistinction, there is very little Al signal in the A layer in the same time span.

4. After 64 h at 900°C (Fig. 10d), four layers, A, B, and C together with a P layer, are now clearly discernable. In contrast to Fig. 10a-c, Fig. 10d was taken in the secondary mode in order to emphasize the morphology of the various layers. Layers A, B, and C to the right of the P plane are relatively dense; the C layer to the left of the P plane, however, is quite porous. The Al signal, as determined by EDS scans (not shown) is strongest at B, and in and near the P layer.

After 16 h of oxidation at 1000°C, the layers are now significantly thicker, (Fig. 11a and b) but their order is similar to those at 900°C (Fig. 10d). Note that the P layer is now significantly deeper within the oxide layer, and much closer to the substrate/oxide interface. Relative to the outermost layer, the other layers are porous (Fig. 11a). At 1000°C, there is no layer that corresponds to the porous C layer to the left of the P plane shown in Fig. 10d. Oxidizing at 1000°C for 64 h results in the morphology shown in Fig. 11c, where two P planes are obvious. The outer P plane is now a clear demarcation line between layer C, and a new layer, which is a two-phase intimate mixture of Al<sub>2</sub>O<sub>3</sub> and TiO<sub>2</sub>. This layer was labeled D in Part I. An important characteristic of the transition is that, while the Ti<sup>4+</sup> ions and O<sup>2-</sup> continue to diffuse across the P layers, for some reason the Al<sup>3+</sup> ions do not. The evidence for this is obvious by comparing Fig. 11a and c: increasing the oxidation time from 16 to 64 h increases the thickness of the A layer from ≈100 μm to 216 μm and creates the D layer, but does not change the thickness of the B layer that remains at ≈50 μm. The reason for the transition from stage II to stage III, *i.e.* Fig. 11b-c, is not clear at this time.

Here, it is useful to think of the B layers as the repository of all the Al ions that are swept out of the C layers. In all micrographs

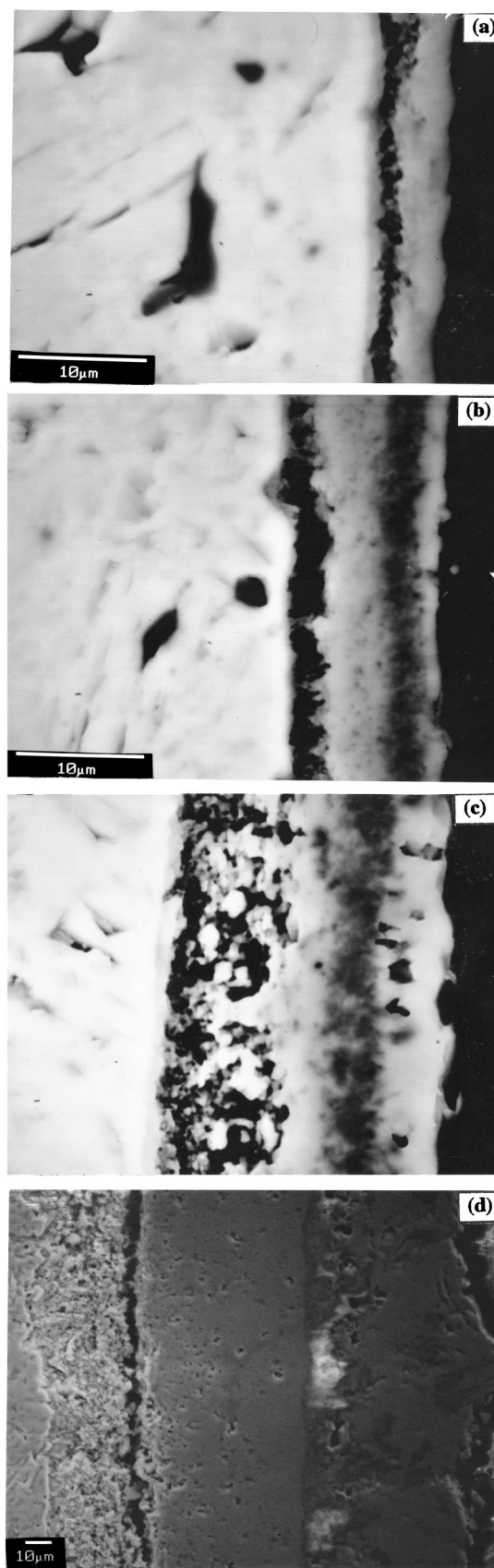


**Figure 10.** Backscattered SEM image of the oxide layers that formed after oxidation of Ti<sub>4</sub>AlN<sub>2.9</sub> at 900°C for (a) 30 min, (b) 1 h, (c) 2 h. Gap present in a and b is being filled, *i.e.*, sintering is occurring in c. (d) Secondary SEM image of sample oxidized at 900°C for 64 h.

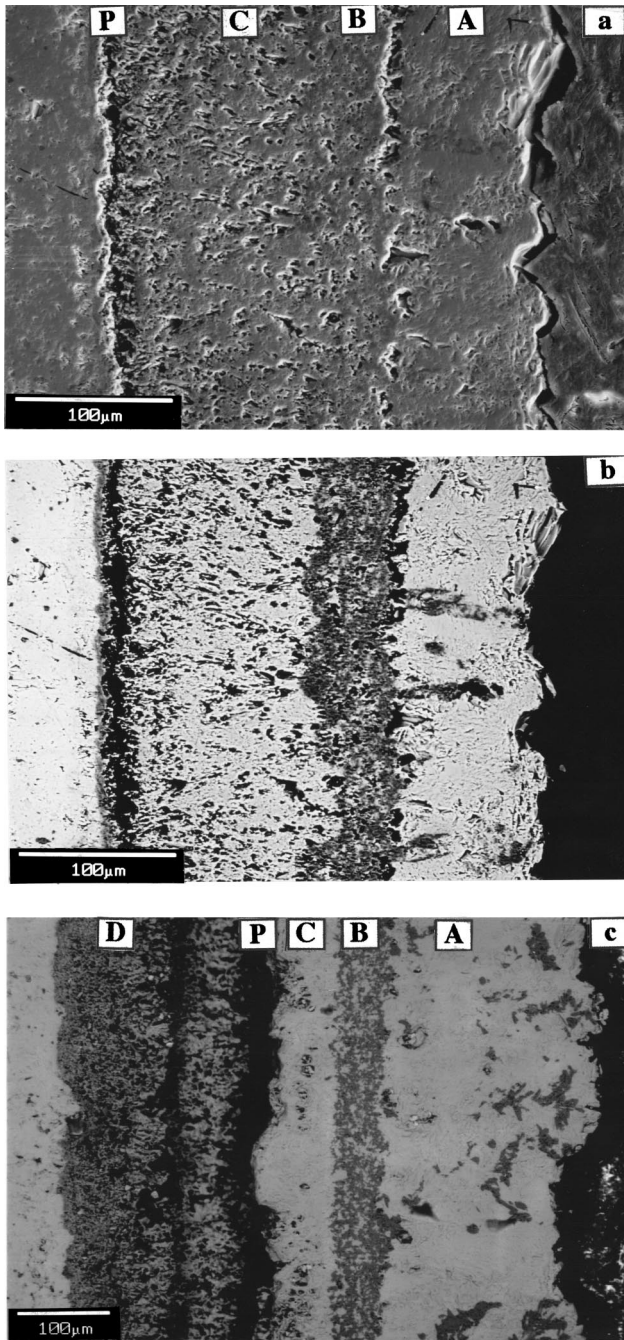


**Figure 11.** Cross-sectional SEM micrographs of a  $\text{Ti}_4\text{AlN}_{2.9}$  sample oxidized in air at (a)  $1000^\circ\text{C}$  for 16 h (secondary mode) showing porosity, (b) backscattered mode showing layering, (c)  $1000^\circ\text{C}$  for 64 h (backscattered mode) showing the formation of more layers.

shown herein, the B layers are always associated with C layers of comparable thicknesses adjacent to them on the lower  $p_{\text{O}_2}$  side (*i.e.*, closer to the substrate side).

After 0.5, 1, and 2 h at  $1000^\circ\text{C}$  (not shown), the oxide scales, while thicker, are morphologically quite similar to those at  $900^\circ\text{C}$ . The gap however, is less pronounced at  $1000^\circ\text{C}$ . After 2 h the C layer is  $\approx 50 \mu\text{m}$  thick, quite porous, and similar in morphology to the C layer shown in Fig. 10c.

Oxidation of  $\text{Ti}_4\text{AlN}_{2.9}$  for 64 h at  $1100^\circ\text{C}$ , results in a striated microstructure (Fig. 12). The order of the layers, from the air/oxide interface inward is A (with  $\text{Al}_2\text{O}_3$  stringers)/C/B/C/P/C/D. Com-

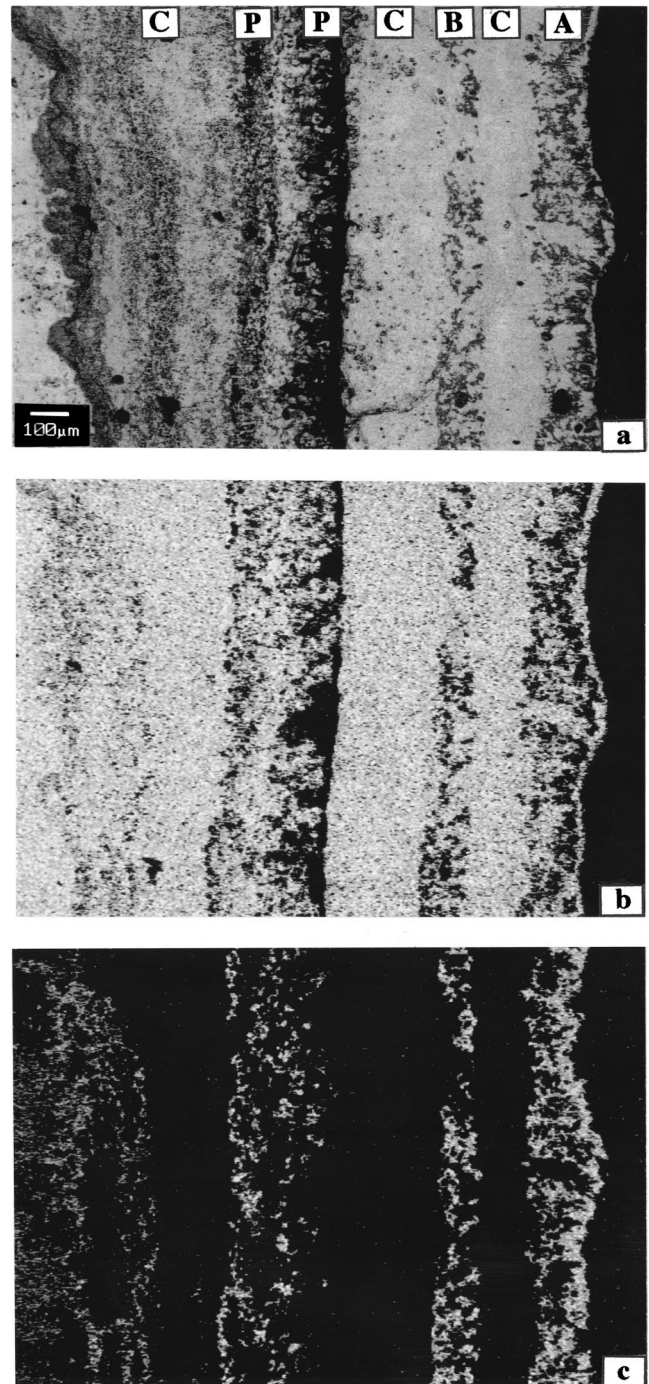


**Figure 12.** Cross-sectional SEM micrographs of a  $\text{Ti}_4\text{AlN}_{2.9}$  sample oxidized in air at  $1100^\circ\text{C}$  for 64 h. (a) Backscattered mode, (b) Ti map, (c) Al map. Dark stained area near substrate/oxide interface is dissociated  $\text{Ti}_4\text{AlN}_{2.9}$  (see also Fig. 17).

paring the Al signal in the outermost layers in Fig. 11c and 12c, it is obvious that higher temperatures induce the  $\text{Al}_2\text{O}_3$  to migrate outward, *i.e.*, toward the air/oxide interface.

In addition, adjacent to the substrate, a stain-like layer is apparent. This layer is a two-phase mixture of  $\text{TiN}_x$  and Al, the origin of which is the dissociation of  $\text{Ti}_4\text{AlN}_{2.9}$  according to<sup>16</sup>



The oxidation then presumably proceeds by the oxidation of the Al

and  $TiN_x$  separately. The  $M_{n+1}AX_n$  phases do not melt, but peritectically decompose into the  $MX_x$  compound and the A group element.<sup>15-19</sup> The decomposition temperature is a function of impurities.<sup>19</sup> In Ar, the dissociation temperature of  $Ti_4AlN_{2.9}$  is in excess of 1400°C.<sup>16</sup> Based on the results shown here, oxygen apparently reduces that decomposition temperature to somewhere between 1000 and 1100°C. The same is also true for  $Ti_3AlC_2$  (see below). This decomposition, for reasons that are not understood, is believed to reduce  $k_x$  compared to what it would have been had there been no decomposition (Fig. 4b, top left). It is for this reason that the 1100°C datum point is not included in calculating the  $k_x$  values for  $Ti_4AlN_{2.9}$ .

$Ti_3AlC_2$ .—Based on XRD of the reaction scales (not shown) the most likely overall oxidation reactions for  $Ti_3AlC_2$  is



The  $x$  vs.  $t$  curves for  $Ti_3AlC_2$ , subject to an analysis identical to the one used to generate Fig. 9, are shown in Fig. 13. Here again, the kinetics appear to change from parabolic early on, to linear at longer times. The anomalous point at 64 h that falls on the dotted line in Fig. 2b is noteworthy; its significance is discussed shortly.

A least-squares fit of the Arrhenius plots of  $k_x$  for  $Ti_3AlC_2$ , yields

$$k_x \text{ (m}^2\text{/s)} = 1.15 \times 10^5 \exp - \frac{443,186 \text{ (kJ/mol)}}{RT} \quad [11]$$

The actual values are listed in Table I in Part I,<sup>1</sup> and plotted in Fig. 4b. Here again because of dissociation, the datum point at 1100°C was excluded from the least-squares fit. From these results it is apparent that  $Ti_4AlN_{2.9}$  is less oxidation resistant than  $Ti_3AlC_2$ , which in turn, is not as good as the 211 phases. Not surprisingly, and in total agreement with the Ti-aluminide literature, increasing the Al content in the substrate enhances the oxidation resistance, presumably because the  $Al_2O_3$  content in the scales increases. Also not surprisingly, the activation energies for  $Ti_4AlN_{2.9}$  and  $Ti_3AlC_2$  are comparable to those of the 211 phases.

Included in Fig. 4b for comparison purposes are the  $k_x$  values for  $Ti_3Al$  available in the literature.<sup>9,13</sup> Despite the sporadic nature of the latter, it is clear that the  $k_x$  values for  $Ti_4AlN_{2.9}$  are comparable to those of  $Ti_3Al$ . In contradistinction, the oxidation resistance of  $Ti_3AlC_2$  is significantly better than its binary counterpart (Fig. 4b). The reason for this state of affairs is speculated on below.

In the 800-1000°C temperature range, the oxide scale thicknesses that form on  $Ti_3AlC_2$  are thinner than, but morphologically similar to, the ones that form on  $Ti_4AlN_{2.9}$ . At 800°C the oxide scale (not shown) is compact and dense, and quite protective. Even after 64 h at 800°C, the oxide scale is less than 10  $\mu\text{m}$  thick. In Fig. 13, the thickness of the scale that formed on the sample oxidized for 64 h at 1000°C was thinner than the one formed after the significantly shorter oxidation of 25 h at the same temperature. It is more important, however, that this datum point appears to fall on the extension of the parabolic kinetics line fit to the short time results (Fig. 13b). A comparison of the two microstructures, shown in Fig. 14a and b, respectively, shed some light on the anomalous behavior of the sample oxidized for 64 h. The simplest explanation is that, for reasons that are not clear, the oxide layers shown in Fig. 14b remained dense and crack free, while the outermost layers that formed after 25 h (Fig. 14a) must have microcracked at some time during the run. Such cracks would introduce oxygen via a parallel path (*i.e.*, not through bulk diffusion) and enhance the oxidation kinetics. In other words, it is postulated that as the layers get thicker, stresses, probably sintering ones, are sufficient to micro- or even macrofracture the layers allowing for a parallel path for oxygen to flow into the interior. Furthermore, and based on this and other evidence presented herein, it appears that the deviation from parabolic kinetics coincides with the onset of demixing; if the latter can be suppressed,

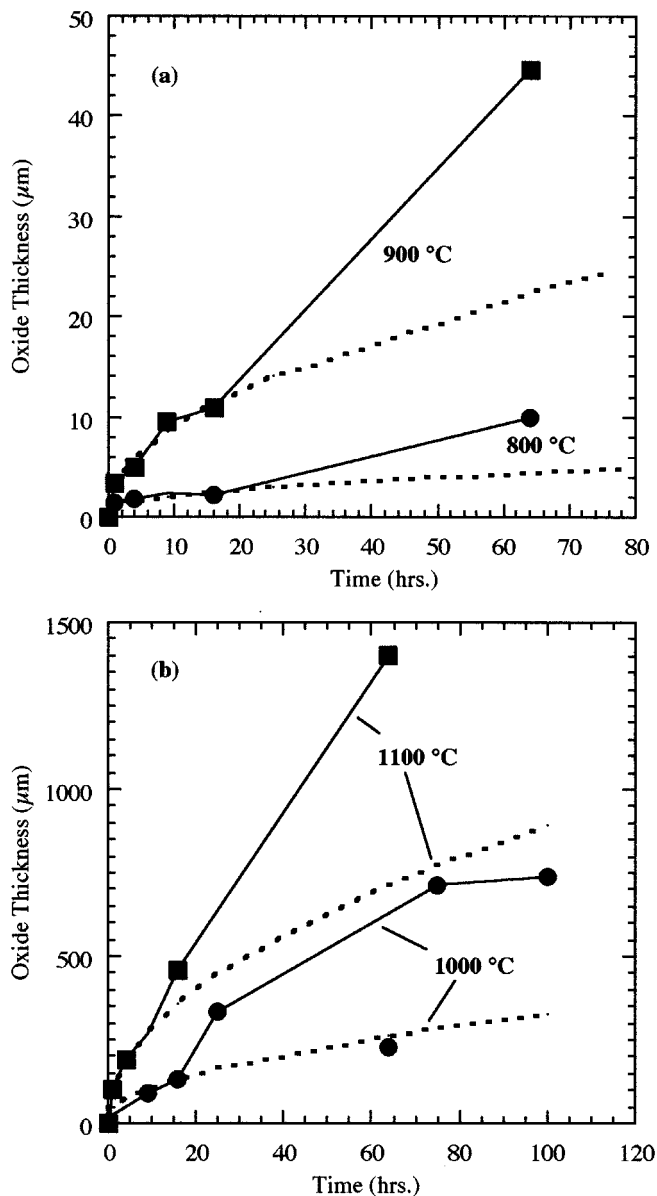


**Figure 13.** Time dependence of layer thickness,  $x$ , formed on  $Ti_3AlC_2$  samples oxidized at (a) 800 and 900°C, and (b) 1000 and 1100°C. The dashed lines represent Eq. 4 in text, plotted using  $k_x$  values obtained from least-squares fits of  $x^2$  vs.  $t$  curves (not shown) at short times (<20 h).

the oxidation resistance of these ternaries and possibly the Ti-aluminide intermetallics could be greatly enhanced.

A dramatic example of the type of microstructure that the repetition of such a process yields is shown in Fig. 15. These micrographs are of a sample heated to 1100°C for 64 h, which resulted in a highly striated microstructure in which  $Al_2O_3$ -rich,  $TiO_2$ -rich, and P layers repeat almost a dozen times. This is an important micrograph because it unequivocally proves that (i) demixing is occurring, and is occurring repeatedly, and (ii) demixing is occurring by having the  $Al^{3+}$  ions diffuse toward the high  $p_{O_2}$  side (in every layer, the  $Al_2O_3$  layer is adjacent to the high  $p_{O_2}$  side). The latter is also seen clearly in most of micrographs shown in this work; in most cases, the volume fraction of the  $Al_2O_3$  islands or streamers in the outermost A layers increase with time (*e.g.*, Fig. 12c). To understand the atomistic mechanisms required for the striations to form refer to Fig. 16, which is an SEM micrograph of a sample that was oxidized at

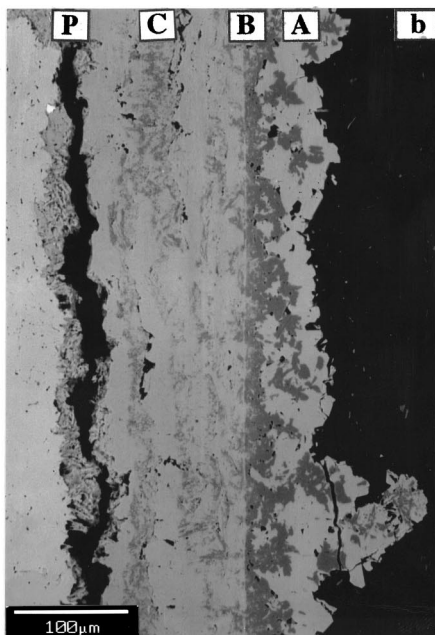
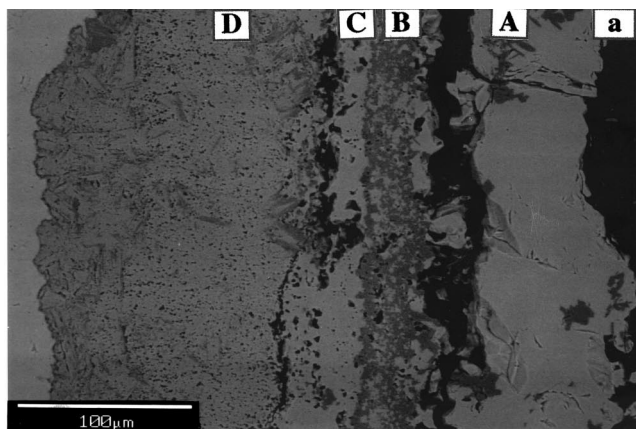


**Figure 14.** Cross-sectional backscattered SEM micrographs of a  $\text{Ti}_3\text{AlC}_2$  sample oxidized in air at  $1000^\circ\text{C}$  for (a) 25 h, and (b) 64 h. The oxide layer thickness for b is less than that for a, despite the significantly longer oxidation time for the former (see text for details).

$1100^\circ\text{C}$  for 16 h. The top few layers are indistinguishable from the ones described so far. However, in this sample, there is a fairly thick ( $\approx 300 \mu\text{m}$ ) D layer, comprised of a fine two-phase mixture of  $\text{Al}_2\text{O}_3$  and  $\text{TiO}_2$ . The  $\text{Al}_2\text{O}_3$  particles are not visible at the magnification of Fig. 16, but are discernable at higher magnifications (not shown). As the oxidation proceeds, the  $p_{\text{O}_2}$  within the P layers must increase to some value at which demixing can occur (*i.e.*, the condition given by Eq. 2 in part I<sup>1</sup> is reached), at which time the  $\text{Al}^{3+}$  ions diffuse toward the high  $p_{\text{O}_2}$  side and precipitate as  $\text{Al}_2\text{O}_3$ . To do so, the  $\text{Al}_2\text{O}_3$  particles in layer D must dissolve at the low  $p_{\text{O}_2}$  side and eventually reprecipitate at the high  $p_{\text{O}_2}$  side. This process must also form vacancies that diffuse inward and ultimately precipitate along a plane, *viz.* the P planes. As noted above, these P planes prevent the further migration of  $\text{Al}^{3+}$  outward, which is why the  $\text{Al}_2\text{O}_3$  particles are invariably clustered at the high  $p_{\text{O}_2}$  side of each segment contained between two P layers. The evidence for this hypothesis is multifold, and includes

1. The change in oxidation kinetics at around 16 h (Fig. 13) from parabolic to a faster oxidation rate. Based on Fig. 15, it is reasonable

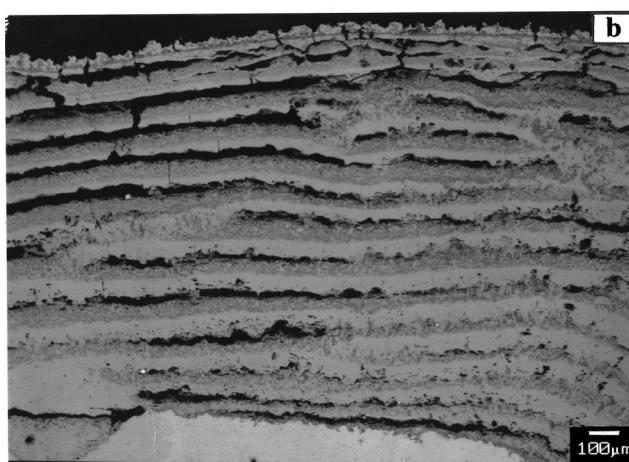
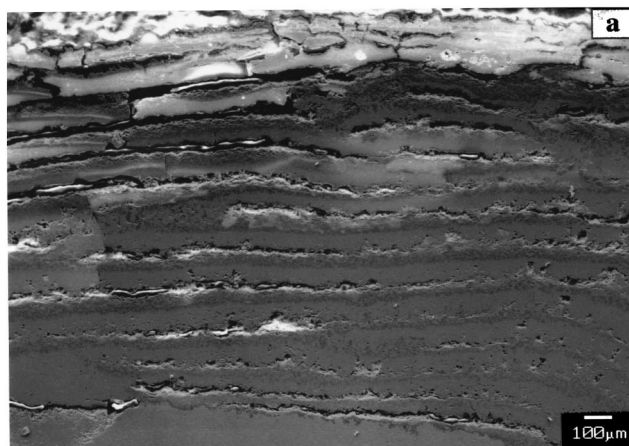


**Figure 15.** Cross-sectional SEM micrographs of a  $\text{Ti}_3\text{AlC}_2$  sample oxidized in air at  $1100^\circ\text{C}$  for 64 h. (a) Secondary mode showing topography, and (b) backscattered mode. Three layers, a bright  $(\text{Ti}_{1-y}\text{Al}_y)\text{O}_{2-y/2}$  layer, a darker  $\text{Al}_2\text{O}_3$ -rich layer, and planes of porosities or P planes, repeat over 10 times.

to assume that the outermost layers, with their many fissures and cracks, are less protective than if they had remained intact.

2. The overall volume fraction of the  $\text{Al}_2\text{O}_3$  in each segment contained between two P layers, is  $\approx 20 \text{ vol } \%$  which is comparable to the theoretical vol fraction ( $\approx 20 \text{ vol } \%$ ) expected from Reaction 10. The volume fraction in the  $\text{Al}_2\text{O}_3$ -rich segment of each striation

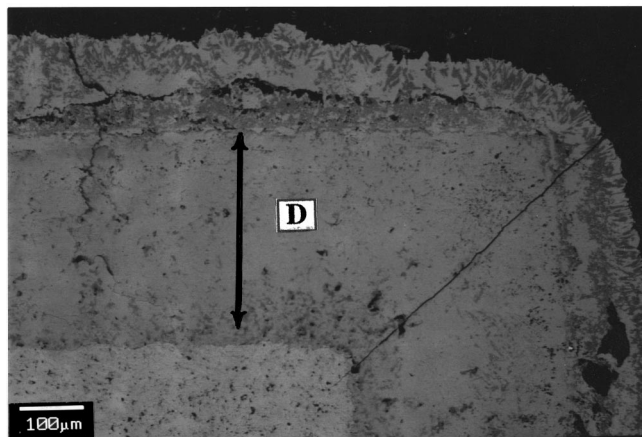


**Figure 16.** Cross-sectional backscattered SEM micrographs of a  $\text{Ti}_3\text{AlC}_2$  sample oxidized in air for 16 h at  $1100^\circ\text{C}$ .

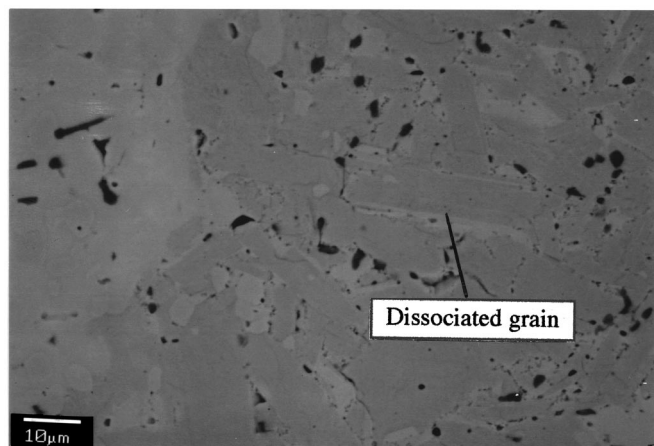


**Figure 17.** Cross-sectional backscattered SEM micrographs of a region near the oxide/substrate interface of a  $\text{Ti}_3\text{AlC}_2$  sample oxidized in air for 64 h at  $1100^\circ\text{C}$ . The topotactical nature of the decomposition that results in  $\text{TiC}_x$  and Al is obvious in some of the grains.

is 50 vol%. In other words, after demixing, the 20 vol %  $\text{Al}_2\text{O}_3$  within each lamella is redistributed and concentrates at the high  $p_{\text{O}_2}$  side.

3. Such a hypothesis is the simplest way to explain how the microstructure shown in Fig. 16 is transformed into the one shown in Fig. 15. It is difficult to conceive of another scenario whereby a homogeneously distributed two-phase mixture (layer D in Fig. 16) is transformed to the heterogeneous striated structure (Fig. 15).

The same decomposition reaction observed at  $1100^\circ\text{C}$  in  $\text{Ti}_4\text{AlN}_{2.9}$  also occurs in  $\text{Ti}_3\text{AlC}_2$  (the decomposition temperature in Ar is  $>1400^\circ\text{C}$ <sup>15</sup>). Once again, this somewhat complicates the sequence of events leading to the formation of the oxide layers, but in this case does not seem to greatly affect the  $k_x$  values. Nevertheless, as noted above, the least squares fit of  $k_x$  (Eq. 11) exclude the datum point at  $1100^\circ\text{C}$ . It is important to note, however, that the end phases are identical, with or without dissociation. Furthermore, the decomposition occurs topotactically by having the Al diffuse out of the basal planes. This is shown in Fig. 17 in which some grains are clearly dissociated while maintaining their original shape. Given that this is one of the preferred modes of reaction for  $\text{Ti}_3\text{SiC}_2$ ,<sup>20,21</sup> these results are not too surprising.

A collateral benefit of this work, and important independent evidence that Al is indeed diffusing in  $\text{TiO}_2$ , is the possibility of estimating the diffusivity of Al,  $D_{\text{Al}}$ , in  $\text{TiO}_2$ , by measuring the width of the C layers, *i.e.*,  $(\text{Ti}_{1-y}\text{Al}_y)\text{O}_{2-y/2}$ , after a given oxidation time. Since the B layers form from the C layers, the width of the latter can be used to crudely estimate  $D_{\text{Al}}$ .<sup>c</sup> For example, in Fig. 11b, the width of the C layer after 16 h at  $1000^\circ\text{C}$  is  $\approx 120 \mu\text{m}$ . This translates to a  $D_{\text{Al}}$  of  $(\sim x^2/2t)$  of  $\sim 1.25 \times 10^{-13} \text{ m}^2/\text{s}$ . An Arrhenius plot of the  $D_{\text{Al}}$  values calculated from the appropriate micrographs at other temperatures and times, for both  $\text{Ti}_3\text{AlC}_2$  and  $\text{Ti}_4\text{AlN}_{2.9}$  is shown in Fig. 18. Also included in Fig. 18, are the literature results for the diffusivity of Al in rutile samples.<sup>22</sup> The agreement between the two sets of results is excellent, especially considering the crude method used to estimate the  $D_{\text{Al}}$  used here. And while this does not prove that Al is diffusing through  $\text{TiO}_2$ , it certainly is consistent with that notion.

<sup>c</sup> Not all micrographs can be used to estimate  $D_{\text{Al}}$ . Two criteria used were that there be only one C layer, and that the oxidation had proceeded for a while. A good example is Fig. 11a, in which a wide C layer that formed after 16 h is clearly visible. This layer must have formed in less than 16 h, and thus, the values reported here are slightly lower than actual. It is important to note that even if the time was, for example, halved to 8 h, that would alter D by a factor of 2, which considering the scale of Fig. 18, and the crude approximation made to calculate  $D_{\text{Al}}$  is almost within the noise level.

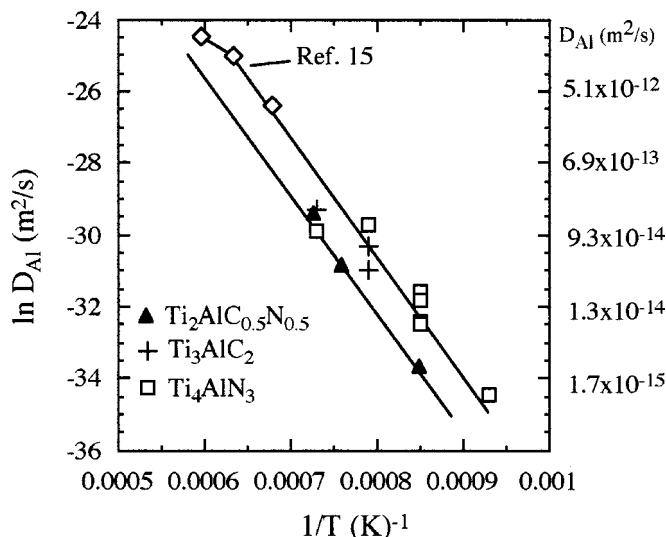


**Figure 18.** Arrhenius plots for the diffusion of Al in rutile determined from this work. Also included are the results of Yan and Rhodes.<sup>22</sup>

Repeating the same exercise using some of the micrographs shown for the 211 phases yields a second series of points that are lower than the first (Fig. 18). At face value, these results are somewhat surprising, since the diffusivity is ostensibly occurring in the same matrix, *i.e.*,  $\text{Al}_2\text{O}_3$ -saturated  $\text{TiO}_2$ , in all cases. The most likely explanation for the discrepancy is that in the case of  $\text{Ti}_4\text{AlN}_{2.9}$  and  $\text{Ti}_3\text{AlC}_2$ , the resulting matrix is not fully dense and other parallel diffusion paths, in addition to bulk diffusion, such as grain boundary, surface, are operative. This is an important observation, and is the most probable explanation for the differences in  $k_x$  between the various ternaries. For reasons that are not clear, the scales that form on the 211 phases must be denser than those that form on  $\text{Ti}_3\text{AlC}_2$ , which in turn are denser than the ones that form on  $\text{Ti}_4\text{AlN}_{2.9}$ . This conclusion is corroborated by much of the microstructural evidence shown in this work. Further evidence for the fact that the aforementioned porosity affects the oxidation kinetics can be gleaned by comparing the oxidation behavior of Ti, the Ti-Al intermetallics, and the ternary compounds. The oxygen diffusivities determined from tracer experiments on fully dense rutile samples are about two orders of magnitude lower than those determined from oxidation experiments, be they on Ti, the ternaries studied here, or Ti-aluminide intermetallics (see Fig. 3, Part I<sup>1</sup>).

Some final comments are in order. The  $M_{n+1}\text{AlX}_n$  phases have several exceptional and mechanical properties, especially at higher temperatures.<sup>14-16</sup> In some cases, they rival the commercially available Ni-based superalloys, especially considering that the densities of the ternaries are roughly half the latter. The results presented in this series of papers, however, make it clear that, before their potential can be fulfilled, their oxidation resistance has to be enhanced, especially at  $T > 1000^\circ\text{C}$ . In this respect, they are not unlike the Ti-aluminide intermetallics.<sup>8</sup> The key here, as it is for the intermetallics, is to so tailor the chemistry and, possibly microstructure, such that an  $\text{Al}_2\text{O}_3$  protective layer forms on the surface. In contrast to the Ti-aluminides, however, one advantage that the  $M_{n+1}\text{AlX}_n$  do possess is that, at least up to 100 h, there is little evidence that they dissolve any measurable concentrations of oxygen, and consequently, are immune from the embrittlement such dissolution engenders in the Ti-aluminide intermetallics.

## Conclusions

The oxidation of reaction HIP polycrystalline samples of  $\text{Ti}_2\text{AlC}$ ,  $\text{Ti}_2\text{AlC}_{0.5}\text{N}_{0.5}$ ,  $\text{Ti}_4\text{AlN}_{2.9}$ , and  $\text{Ti}_3\text{AlC}_2$  in air, in the  $800\text{--}1100^\circ\text{C}$  range occurs by the inward diffusion of oxygen and the outward

diffusion of Al and Ti ions through a rutile-based solid solution, viz.,  $(\text{Ti}_{1-y}\text{Al}_y)\text{O}_{2-y/2}$  in which  $y < 0.05$ . The fate of the C and/or N is unknown, but is presumed to diffuse outward through the layers and oxidize. If the  $p_{\text{O}_2}$  is relatively low, both oxides can coexist. However, as the oxidation proceeds and the  $p_{\text{O}_2}$  increases, demixing occurs with the  $\text{Al}_2\text{O}_3$  migrating to the high  $p_{\text{O}_2}$  side. This process occurs by the dissolution and reprecipitation of  $\text{Al}_2\text{O}_3$  particles through the  $(\text{Ti}_{1-y}\text{Al}_y)\text{O}_{2-y/2}$  matrix and results in the formation of layers of high porosity. The final microstructure is characterized by the presence of multiple striated layers in which layers of  $\text{TiO}_2$ , almost totally denuded of  $\text{Al}_2\text{O}_3$ , alternate with  $\text{Al}_2\text{O}_3$ -rich layers and layers of porosity. The onset of demixing coincides with the deviation of the oxidation kinetics from parabolic to linear. The microstructural observations are in agreement with the model presented in Part I,<sup>1</sup> in which it was concluded that the diffusion of O and/or Ti through the  $(\text{Ti}_{1-y}\text{Al}_y)\text{O}_{2-y/2}$  layer is rate limiting.

Both  $\text{Ti}_4\text{AlN}_{2.9}$  and  $\text{Ti}_3\text{AlC}_2$  decompose in air at 1100°C into Al and the  $\text{TiN}_x$  or  $\text{TiC}_x$  just below the oxide layers that form. This decomposition, which occurs topotactically, does not affect the final morphology or the sequence of the layers that form, but slightly affects the  $k_x$  values, especially for  $\text{Ti}_4\text{AlN}_{2.9}$ .

#### Acknowledgment

This work was partially supported by the U.S. Army Research Office (DAAD19-00-1-0435) and partially by the National Science Foundation (DMR-0072067).

*Drexel University assisted in meeting the publication costs of this article.*

#### References

1. M. W. Barsoum, *J. Electrochem. Soc.*, **148**, C522 (2001).
2. M. W. Barsoum, T. El-Raghy, and L. Ogbuji, *J. Electrochem. Soc.*, **144**, 2508 (1997).
3. P. Kofstad, *Nonstoichiometry, Diffusion and Electrical Conductivity in Binary Metal Oxides*, p. 142, R. E. Krieger Publications Company, Malabar, FL (1983).
4. P. Kofstad, *High Temperature Oxidation of Metals*, Wiley Interscience, New York (1966).
5. K. Hauffe, *Oxidation of Metals*, Plenum Press, New York (1965).
6. G. Bertrand, K. Jarraya, and J. M. Chaix, *Oxid. Met.*, **21**, (1983).
7. J. Unnam, R. N. Shenoy, and R. K. Clark, *Oxid. Met.*, **26**, 231 (1986).
8. M. P. Brady, B. A. Pint, P. F. Tortorelli, I. G. Wright, and R. J. Hanrahan, Jr., in *Corrosion and Environmental Degradation*, Vol. II, R. Cahn, P. Haasen, and J. Kramer, Editors, Wiley-VCH, Weinheim, Germany (2000).
9. G. Welsch and A. I. Kahveci, in *Oxidation of High Temperature Intermetallics*, T. Grobstein and J. Doychak, Editors, Minerals and Materials Society, Warrendale, PA (1989).
10. G. H. Meier and D. Appalonia, in *Oxidation of High Temperature Intermetallics*, T. Grobstein and J. Doychak, Editors, p. 185, Minerals and Materials Society, Warrendale, PA (1989).
11. Y. Shida and H. Anada, *Mater. Trans., JIM*, **34**, 236 (1993).
12. T. K. Roy, R. Balasubramaniam, and A. Gosh, *Metall. Mater. Trans. A*, **27**, 3993 (1986).
13. J. S. Wu, L. T. Zhang, F. Wang, K. Jiang, and G. Qiu, *Intermetallics*, **8**, 19 (2000).
14. M. W. Barsoum, M. Ali, and T. El-Raghy, *Metall. Mater. Trans. A*, **31**, 1857 (2000).
15. N. Tzenov and M. W. Barsoum, *J. Am. Ceram. Soc.*, **83**, 825 (2000).
16. A. T. Procopio, T. El-Raghy, and M. W. Barsoum, *Metall. Mater. Trans. A*, **31**, 373 (2000).
17. M. W. Barsoum, G. Yaroshuck, and S. Tyagi, *Scr. Mater.*, **37**, 1583 (1997).
18. L. Farber and M. W. Barsoum, *J. Mater. Res.*, **14**, 2560 (1999).
19. N. Tzenov, M. W. Barsoum, and T. El-Raghy, *J. Eur. Ceram. Soc.*, **20**, 801 (2000).
20. M. W. Barsoum, T. El-Raghy, L. Farber, M. Amer, R. Christini, and A. Adams, *J. Electrochem. Soc.*, **146**, 3919 (1999).
21. T. El-Raghy and M. W. Barsoum, *J. Appl. Phys.*, **83**, 112 (1998).
22. M. F. Yan and W. W. Rhodes, *J. Appl. Phys.*, **53**, 8809 (1982).